

Published in final edited form as:

*J Struct Biol.* 2011 April ; 174(1): 203–212. doi:10.1016/j.jsb.2010.11.027.

## Self-aligning amelogenin nanoribbons in oil-water system

Xiaodong He, Shenping Wu<sup>#</sup>, Olga Martinez-Avila, Yifan Cheng<sup>#</sup>, and Stefan Habelitz

Department of Preventative and Restorative Dental Sciences, University of California, San Francisco

<sup>#</sup> Department of Biochemistry & Biophysics, University of California, San Francisco

### Abstract

The highly organized microstructure of dental enamel is a result of protein-guided anisotropic growth of apatite nanofibers. It is established that amelogenin proteins, the main constituent of the developing enamel matrix, form nanospheres in vitro, but the amphiphilic nature of the full-length protein conveys the possibility of generating more complex structures as observed with other surfactant-like molecules. This study tested if the use of metastable oil-water emulsions can induce supramolecular assemblies of amelogenin. Recombinant full-length amelogenin, rH174, was mixed into octanol/ethyl acetate preparations of different ratios to form emulsions at pH 4.5 and 7.4. Atomic force and electron microscopy showed the formation of  $16.7 \pm 1.0$  nm wide nanoribbons which grew to several micrometer length over a period of days. Nanoribbons formed from reverse micelles by enabling hydrophobic tails of the molecules to interact while preventing the formation of amelogenin nanospheres. Ribbon formation required the presence of calcium and phosphate ions and may be localized at a dark central line along the amelogenin ribbons. The ribbons have a strong tendency to align in parallel maintaining 5 to 20 nm space between each other. The growth rates and number of ribbons were significantly higher at pH 4.5 and related to the metastability of the emulsion. A model for ribbon extension proposes the addition of short segments or amelogenin dimers to the ends of the ribbon. The formation of self-aligning and uniaxially elongating amelogenin structures triggered by the presence of calcium and phosphate may represent a suitable new model for protein controlled mineralization in enamel.

### Keywords

Amelogenin; dental enamel; self-assembly; atomic force microscopy; electron microscopy; emulsion

### Introduction

Self-assembly guides biological organization, is ubiquitous throughout life chemistry and occurs at many length-scales in nature. The formation of a tissue or organ is a hierarchical process with several tiers of self-assembling steps (Monnard and Deamer, 2002). In the case of the enamel matrix, its main component, amelogenin proteins are known to assemble into nanospheres (Fincham et al., 1995; Robinson et al., 1981). The full-length amelogenin protein is a bipolar molecule that is hydrophobic over most of its length, but contains hydrophilic amino acids at the C-terminus. Bipolarity is also a prerequisite for the self-

---

**Publisher's Disclaimer:** This is a PDF file of an unedited manuscript that has been accepted for publication. As a service to our customers we are providing this early version of the manuscript. The manuscript will undergo copyediting, typesetting, and review of the resulting proof before it is published in its final citable form. Please note that during the production process errors may be discovered which could affect the content, and all legal disclaimers that apply to the journal pertain.

assembly of synthetic materials that can generate a large variety of nanostructures, including fibers, tubes, sheets or membranes and rods (Claussen et al., 2003; Colfen and Mann, 2003; Elie-Caille et al., 2005; Hartgerink et al., 2001; Lindoy and Atkinson, 2000). Some artificial systems also succeeded in generating larger structures through hierarchical self-assembly of the primary nanoconstruct (Choi et al., 1999; Yan et al., 2004).

Self-assembly of amelogenin into nanospheres appears to be dominated by its hydrophobic residues that tend to associate at the non-polar regions and thus shield themselves from the surrounding water (Fincham et al., 1995; Moradian-Oldak, 2001). Amelogenin self-assembly has been studied to a large extent *in-vitro*, but due to the absence of this protein in the developed and erupted tooth, investigations were typically performed with recombinant proteins. The size of nanospheres from full-length amelogenin is polydisperse and varies with temperature, concentration, pH, ionic environment and time (Margolis et al., 2006; Moradian-Oldak et al., 2000). In addition, solubility of amelogenin in aqueous solutions is limited. The solubility is strongly dependent on the pH (Tan et al., 1998). Studies on the molecular self-assembly of amelogenin have been performed to a large extent by dynamic light scattering (DLS), atomic force and electron microscopy. At this point it is widely accepted that the full-length protein forms nanospheres of about 15 to 40 nm in diameter under physiological conditions *in-vitro* and at concentrations below the solubility limit (Moradian-Oldak, 2001). A core-shell model for the nanospheres has been proposed, where hydrophilic and negatively charged side chains prevent the agglomeration of hydrophobic cores of the nanospheres (Aichmayer et al., 2005). Recent studies have shown increasing evidence that the full-length protein has the capacity to form chain-like structures consisting of 5 to 10 nanospheres connected to each other like beads on a string (Aichmayer et al., 2005; Beniash et al., 2005; Wiedemann-Bidlack et al., 2007). The string-like nanosphere aggregates were also observed to align themselves parallel to the c-axis of apatite crystals (Habelitz et al., 2004). The aggregation processes were dependent on the pH and appeared to produce organized tertiary structures when approaching the isoelectric point of the protein (Wiedemann-Bidlack et al., 2007). A recent small angle x-ray scattering study showed that nanospheres are actually ellipsoidal and thus may not be isotropic, a possible prerequisite to forming chain-like structures (Aichmayer et al., 2010). Mesh-like networks of full-length amelogenin were also formed during the electrolytic deposition of apatite suggesting that the presence of calcium was a key-factor in the nanochain formation of the protein (Fan et al., 2007). In TEM studies in combination with turbidity measurements a transition from individual nanospheres to string-like arrangements were observed within 150 minutes of sample preparation (Wiedemann-Bidlack et al., 2007), but only if the protein contained both the hydrophilic and the hydrophobic portions. MMP-20 cleavage products of amelogenin lack the hydrophilic portion and have a lower tendency to form chain-like aggregates (Kwak et al., 2009).

The observation of a transition from a nanosphere to string-like arrangements requires kinetic energy for movement and reorganization of the spheres and chain length increases with incubation time. AFM studies have shown that numerous strings of amelogenin can form over a period of days or week and lead to the formation of featureless fibers that lack the pattern of the initial nanospheres, also indicating that the nanosphere may not be the thermodynamically most stable structure amelogenin prefers to maintain (He et al., 2008). The kinetics for such fibrillogenesis was significantly improved when a mixed population of amelogenins containing the full-length protein (rH174) and the MMP-20 cleavage product (rH163) were used and supported the hypothesis that surface charges are involved in controlling the hierarchical assembly of amelogenin (He et al., 2008). Zeta-potential measurements showed values of 6.8 as the isoelectric point of the full-length molecule which coincides well with the increased tendency for aggregation around this pH (Uskokovic et al., 2010). Surface charges are critical in self-assembling systems and have

been fundamental for the design of self-assembling peptide amphiphiles. Several studies in the Stupp laboratory have shown the relevance of the pH to induce supramolecular self-assembly and gelation of peptide amphiphiles. Gelation occurred when the attractive Van der Waals forces overcame the electrostatic repulsion between the counterion double-layer that surrounded a particle or molecule (Stendahl, 2006).

Oil-water mixtures are ubiquitous in nature and are particularly important in biology and industry (Leunissen et al., 2007) When oil and water are mixed, microemulsions develop either by the formation of micrometer sized oil-droplets or micelles dispersed in a supersaturated ionic aqueous solution or in the inverse system based on reverse micelles where water droplets form and are stabilized by the use of surfactants e.g. AOT [sodium bis-(2-ethylhexylsulfo succinate)] surfactants or DDAB [didodecylidimethyl-ammonium bromide]. Such microemulsions have been used to create unique crystal morphologies at the nanometer scale (Colfen and Mann, 2003; Qi et al., 2001). Several studies were successful in controlling the growth of inorganic materials, including calcium phosphates, by forcing the crystals to adapt the micelle or the intermicellar structure (Chen et al., 2007). Walsh and Mann were able to produce interconnected fibrous apatite crystals using DDAB in an oil-water system at temperatures below the melting point of the oil phase (Walsh and Mann, 1995). Margolis et al. reported that a calcium phosphate material with structural features resembling tooth enamel (bundles of co-aligned filaments) was synthesized from a highly viscous reaction solution containing reverse micelles and micro-emulsions, stabilized by AOT (Margolis et al., 2006). That study also emphasized the analogies between the action of the surfactant and the amphiphilic protein amelogenin.

In contrast to a regular micelle, the reverse micelle is defined by the hydrophilic portion of the surfactant being at the interior of the micelle which contains water, while the hydrophobic portion is exposed to the surrounding non-polar matrix or oil phase. Reverse micelles, thus, provide a restrictive aqueous environment for controlled chemical or biological reactions and have been depicted as passive nano-reactors (Uskokovic and Drofenik, 2007). Reverse micelles may have been the precursors to the formation of membranes of a biological cell. They are also critical in current approaches for the immobilization and encapsulation of macromolecules for medical and pharmaceutical purposes (Trivedi and Kompella, 2010) and have been used for protein extraction through the affinity partitioning process (Kelley et al., 1993).

This study used an oil-water system in which full-length amelogenin molecules play the role of the surfactant. Different compositions of the oil phase were used and the pH of the ionic solutions was adjusted until metastable emulsions formed. When analyzed by TEM and AFM elongated, ribbons of 16.7 nm width composed of recombinant full-length amelogenin molecules formed in such emulsion. A model for the process of self-assembly is described.

## 2. Materials and Methods

The full-length human amelogenin protein (rH174) was obtained via recombination and expression in BL21(DE3) plysS *E. Coli*, as described previously (Li et al., 2003). The protein was purified by incubating the extract with C4 hydrophobic beads in 30% acetonitrile with 0.1% trifluoacetate (TFA) for 30 min at room temperature. After washing, the protein was eluted by 80% acetonitrile in 0.1% TFA and lyophilized to obtain aliquots of about 1mg rH174 per test-tube. Amelogenins rH174 were dissolved in double deionized water to prepare different concentration of stock solutions according to experimental demand. Stock solutions of calcium chloride dehydrate and potassium dihydrogen phosphate were prepared from reagent grade chemicals. The molar ratios of the solution components were varied in a series of experiments. Octanol (99% reagent grade, Fisher Scientific Inc)

and ethyl acetate (99.7+% reagent grade, Fisher Scientific Inc) were used as received. Sodium azide was added to all reaction solutions at 0.02 vol%.

### Preparation of amelogenin stabilized emulsion

For preparing amelogenin stabilized water-in-oil emulsion, the choice of the oil phase is the first step and is based on the principle of like dissolves like. Octanol was chosen as primary oil phase composition due to its low Hildebrand solubility parameter  $\gamma$  of 21.1 (J/cm<sup>3</sup>)<sup>0.5</sup> (Sepassi and Yalkowsky, 2006). Ethyl acetate was used to modify the interfacial tension at the oil-water interface during amelogenin self-assembly (vanBuuren et al., 1996). The addition of ethyl acetate, which most likely acts as a co-surfactants, was required for emulsification as indicated by a creamy white or turbid protein/water/oil mixtures that formed after vortexing. Ethyl acetate (EA) concentrations were adjusted between ratios of 9:1 and 6:4 for Vol<sub>octanol</sub>: Vol<sub>EA</sub> to achieve stability of the emulsion. Emulsion remained turbid for extended time at a volume ratio of octanol and ethyl acetate equal to 7/3, oil-water ratio equal to 4/1 and acidic pHs. With increasing the pH to 7.4 the emulsion stabilized significantly and we did not observe a significant phase separation after 48 hours. After seven days only a small rim of separated water was visible. The final concentration of 3.7 mg/ml of amelogenin rH174 was used in all experiments. The protein concentration is based on the assumption that the protein is distributed in the water phase only and not in the oil phase. Raman spectroscopy confirmed the absence of protein in the oil phase.

### Preparation of filament bundles

In a typical preparation, 125  $\mu$ l of a stock solution of amelogenin was added to 500  $\mu$ l non-polar solution. The oil used was octanol to which different ratios of ethyl acetate were added up to a ratio of 6:4. Oil and protein mixture are defined as solution I. 125  $\mu$ l of calcium stock solution were added to the solution I and 125  $\mu$ l of phosphate stock solution to another test tube with solution I. These two solutions were vortexed separately at 900 rpm for 60 seconds. Then, the phosphate solution was added to the calcium solution and the mixture was vortexed again for 60 seconds along with adjusting pH with Tris/HCl to 7.4, and Bis-tris/HCl to 4.5 or KOH/HCl as necessary. The pH was measured using a calibrated micro glass-electrode (Orion 8220 BNWP, Thermo Electron Co.). Calcium and phosphate concentration was decreased at pH 7.4 to maintain the degree of saturation (DS) for hydroxyapatite in the metastable range. The final concentrations were 33.1 mM CaCl<sub>2</sub> and 20.9 mM KH<sub>2</sub>PO<sub>4</sub> (DS = 3.6) at pH 4.5 and 3.3 mM CaCl<sub>2</sub> and 2.1 mM KH<sub>2</sub>PO<sub>4</sub> (DS = 13.7 at pH 7.4). Suspensions were evaluated for the formation of emulsions which was indicated by a milky white appearance. Emulsions were incubated at 37 °C for different times up to two weeks. Sample-solutions of 20  $\mu$ l were pipetted onto microscope glass slides and kept for one hour in a wet cell to immobilize products onto glass slide avoiding evaporation. Subsequently, solutions were washed off with of few drops of deionized water, immediately dried with dust-free canned air and studied using AFM, SEM and Raman spectroscopy as previously described (He et al., 2008).

### Characterization

The microstructure of the immobilized products was observed using atomic force microscopy (AFM) (Nanoscope III; Digital Instruments, Santa Barbara, CA, USA). Images were obtained in dry conditions using tapping mode with a Si-tip ( $r < 10$  nm, 1 ~ 125  $\mu$ m) (Tap 300, Budgetsensors) at a resonance frequency of ~300 kHz. Si-tips with tip radius of about 5 nm (Nanoworld, SSS-NCH, Switzerland) were used for high resolution images with scan sizes of 1  $\mu$ m or smaller. The average sizes were measured from the AFM graphs using Nanoscope software and determining the average value of at least 50 points. Values were corrected for tip broadening assuming a tip radius of 5 nm. The average aspect (L/W)

ratio of nanostrings was calculated from the mean length and the average diameter of nanostrings.

For TEM imaging, a drop of 2.0  $\mu\text{l}$  sample was applied to a carbon coated copper grid (Electron Microscopy Sciences, USA; Ted Pella, Inc., USA) treated by glow discharge or ultraviolet light which makes the carbon film hydrophilic. After 60 sec. of adsorption, the grid was washed off by two drops of water and air dried. For negative staining, the TEM grid was stained with a 0.75% uranyl formate solution (Electron Microscopy Sciences, USA) following established procedure (Ohi et al., 2004) or a 2% methylamine tungstate solution (NANO-W<sup>TM</sup>, Nanoprobes, USA) after being washed off by water. Grids were imaged with an FEI Tenai 12 TEM (FEI company, USA) at 120kV. Data were acquired with a 4k  $\times$  4k Gatan UltraScan CCD camera (Gatan, Inc., USA). Data for further image processing (e.g. Figure 3) were recorded at defocus around 1.5 $\mu\text{m}$ , and a pixel size of 4.154 Å. The EMAN boxer methodology (Ludtke et al., 1999) (was used to select 604 particles along strings in Figure 3b. The box size was 160  $\times$  160 pixel with an overlap of 40 pixels between adjacent particles along the string axis. Alignment and averaging were carried out using Spider software (Frank et al., 1996)

The localized surface morphology and chemistry of the products were assessed by means of SEM coupled with energy dispersive spectroscopy (EDS), which were implemented on a Hitachi S-4100 system with beam energy of 15.0 keV. Micro-Raman spectroscopy was performed with a 20-mW He-Ne laser at a wavelength of 632.8 nm (HR 800, Jobin Ivon, Horiba Group, Tokyo, Japan) through an 50X objective to obtain spectra in the range from 800 to 1800  $\text{cm}^{-1}$ . The spatial resolution was approximately 4  $\mu\text{m}^2$ . Spectra were obtained at five different spots of each specimen with collection times of 100s and averaged over three scans. CCD-detector was calibrated using a silicon wafer as standard.

The measurements of the average particle size of the aqueous portion of the oil-water emulsions of amelogenin were carried out by a Zetasizer Nano-ZS dynamic light- scattering (DLS) analyzer (Malvern Instruments Ltd., Malvern, Worcestershire, UK). Samples ( $n > 3$ , including various batches) of 1.5 mL (total volume) were analyzed for particle size in multiple runs, at 37°C. Each datapoint was the result of averaging over 50 acquisitions, each lasting 10 sec. The particle sizes reported presented hydrodynamic diameters derived from the time-correlation function of the particle number density (Berne and Pecora, 1974).

## Results

Amelogenin oil-water emulsions were prepared with the goal to obtain stable or metastable emulsions. When protein solutions at pH 4.5 and 7.4 were mixed with octanol only, no emulsion formed and water and oil phase separated instantly after the vortexing step. The addition of ethyl acetate stabilized the emulsion significantly at both pH used. The ratio of ethyl acetate to octanol was varied between 1:9 and 4:6 (v/v). A ratio of 3:7 resulted in the longest lasting stability of the emulsion and was used in all experiments described below. There was a significant difference in the time to completely phase separate between samples prepared at pH 4.5 and 7.4. Figures 1a to c show how the emulsion prepared at pH 4.5 gradually phase separated. Emulsification was indicated by a creamy, milk-like appearance of the suspension. At pH 4.5, evidence of phase separation can be observed after about two hours of incubation at 37°C (Fig 1b). The emulsion was completely split into the two components after 24 to 48 hours. A thin whitish looking interface remained between the two phases (Fig. 1c). Emulsions prepared at pH 7.4 were very stable. They did not show signs of phase separation during an initial two days of incubation, but were still predominantly milky-white in appearance at the end of the incubation period of 14 days. Particle size analysis in the water portion of the emulsion formed at pH 4.5 was assessed by DLS (Fig.

1d) over a period of seven days. Initially, big particles which were out of the measurable range were detected. Particles size decreased continuously and reached about 2  $\mu\text{m}$  at day three, and became as low as 30–100 nm between days four and six. After six days the particle size showed a broad variability and was increased for some particles to several micrometer but also showed nanometer sizes for other measurements.

Figure 2 shows TEM analysis of a comparison of amelogenin assemblies formed in a water control system (Figs 2a – c) and in an oil-water system (Figs 2d–f) at incubation times of up to 7 days. The control samples revealed the presence of the characteristic amelogenin nanosphere of about 25 nm in diameter at one day of incubation (Fig 2a). The spheres occasionally associated with each other and formed elongated chain-like structures over a period of 2 to 7 days (Figs. 2b and c). In contrast, when aqueous amelogenin solutions were mixed into an oil phase at equal volumes, ribbon-like structures appeared within hours (Fig. 2d). Later time points showed higher concentrations of ribbons which were also oriented in a parallel fashion (Fig. 2e). With time ribbons also had a tendency to form aggregate into larger fiber-like structures up to 1  $\mu\text{m}$  width and several micrometers in length. Figure 3 shows a TEM image of an amelogenin assembly obtained after 7 days from the oil-water interface. It shows that the elongated structures are ribbons as is evident at locations when the ribbon twists or turns. The ribbons have fairly consistent width of  $16.7 \pm 1.0$  nm as determined by TEM, with the variation being mainly related to orientational misalignments and variations in the staining. AFM analysis showed an average width of 22.1 nm. The increased width in the AFM can be attributed to the tip broadening effect. Since tip radius was about 5 nm, AFM and TEM measurements correspond very well. The height or thickness of the nanoribbons was measured as  $3.1 \pm 0.6$  nm from AFM data.

In areas of low density, ribbons are commonly well aligned and at the same time separated by a narrow spacing of 5–20 nm (Figs. 2, 4, 5 and 6). Figure 4 shows a more detailed analysis of the structure within each ribbon. Stained, positively and negatively stained samples were compared. While the overall orientation of the molecules within the ribbons was not obviously, a dark central line running at the long axes of the ribbons could be identified. This line indicated less transparency for the electron beam which is a result of higher electron density in this region. Averaging over 500 equally sized ribbon segments using TEM software (Frank et al., 1996) provided increased evidence for the dark central line and also revealed further details on the molecular arrangements within the ribbons. AFM analysis of the ribbons was performed at multiple corresponding time points for both pH used in the study (Fig. 5). Ribbons of similar width were observed early on at the oil-water interface and the underlying water phase for pH 4.5 only (Fig. 5a). At pH 7.4 ribbons were observed as early as at three days of incubation (Fig. 5d). With increasing incubation time ribbons became more abundant. The length of the ribbons also increased while at the same time shorter ribbons appeared. Overall ribbons were more abundant for emulsions prepared at pH 4.5 (Fig. 5b) versus pH 7.4 (Fig. 5e). Only at pH 4.5 large accumulations of ribbons were observed at later time points (Fig. 5c) whereas emulsion at higher pH did not show immobilized protein in large quantities (Fig. 5f). When deposited on a glass slide for AFM analysis, ribbons showed good alignment when they were short in length (below 1 $\mu\text{m}$ ). Their degree of organization decreased with increasing ribbon length.

When SEM analysis was performed large amounts of fibrillar structures were frequently observed at pH 4.5. Figure 6a is a SEM micrograph of amelogenin nanoribbons assembled in an oil/water system at pH 4.5 with 33.1 mM  $\text{CaCl}_2$  and 20.9 mM  $\text{KH}_2\text{PO}_4$ . The EDX analysis of this sample detected predominantly the ions of the underlying glass substrate (Si, Na, Al, K) and shows small intensities for calcium and phosphate ions which were used in the assembly process (Fig. 6b). Dense meshworks of randomly distributed amelogenin nanoribbons were also observed by AFM (Fig. 6c). Micro-Raman spectroscopy was

performed on samples that showed crowded layers of amelogenin ribbons as observed by SEM or AFM and recognizable by the confocal microscope of the micro-Raman system used. The obtained spectra were compared to spectra from lyophilized powder of rH174, as received (Fig. 6d). Both Raman spectra showed the characteristic Raman active bands of amelogenin, including a strong band at  $1005\text{ cm}^{-1}$  attributed to phenylalanine and broader bands around  $1450\text{ cm}^{-1}$  and  $1650\text{ cm}^{-1}$  which are attributed to the vibrational modes amide II and I, respectively. Spectra obtained from the amelogenin ribbons appeared more pronounced in the amide I region and showed a shift of the main broad band spanning from  $1655$  to  $1670$  in the lyophilized sample to a sharper peak with a maximum at  $1670\text{ cm}^{-1}$  and a shoulder at  $1645\text{ cm}^{-1}$  after assembly. In addition a peak at  $1607$  was identified after assembly, which appeared as a broad band in the lyophilized powder. The peak at  $1620\text{ cm}^{-1}$  has previously been assigned to the presence of tyrosine residues (Lefevre et al., 2007).

The turbid appearance of the emulsion suggests the formation of reverse micelles, which are only stable for a short period of time and gradually phase separate. Samples were extracted from early time points of the experiment (1 to 20 min). By depositing droplets of  $20\text{ }\mu\text{l}$  of solution onto glass slides we were able to observe circular structures of about  $200\text{--}300\text{ nm}$  in diameter using the AFM (Fig. 7). These structures may be associated with the presence of micelles which in their original form in solution may have been only a few tens of nanometer wide before being plated onto the glass slide.

## Discussion

The full-length amelogenin protein is an amphiphilic or bipolar molecule composed of a hydrophobic core of about 160 amino acids and a hydrophilic head of about 15 acidic and charged residues at the c-terminus. The hydrophobicity of amelogenin strongly dominates its intra- and intermolecular interactions in aqueous solutions which ultimately dominate its self-assembly behavior. The formation of nanospheres of 20 to 40 nm is commonly observed when assembly is performed under aqueous conditions in-vitro and is attributed to hydrophobic forces which direct the molecules to arrange each other in a configuration which keeps the hydrophobic portions away from the surface while the hydrophilic tails are exposed to the water limiting uncontrolled aggregation of the protein (Aichmayer et al., 2005).

As shown in model systems, different pathways of protein folding and subsequent intermolecular interactions and assembly can be achieved if the hydrophobic portion of the protein is prevented from folding by exposing it to an oil phase (Nicholls et al. 1991). A reverse micelle system based on water in oil emulsion was applied with amelogenin playing the role of the surfactant which stabilizes the micelle arrangement. In the presented study we were able to generate emulsions by mixing aqueous suspensions of the amelogenin protein rH174 with a non-polar octanol/ethyl acetate solvent. The composition of the oil phase was critical with respect to stability of the emulsion. A ratio of 3:7 for ethyl acetate to octanol produced emulsions that phase separated over approximately 24–48 into two phases at pH 4.5 (Fig. 1). The oil: water ratio was 4:1 and emulsions were composed of water-droplets (Fig. 1d) stabilized by the presence of the full-length amelogenin protein rH174 dispersed in an oil phase. Hence amelogenin acted as a surfactant and stabilized the polar liquid phase forming a reverse micelle. Micelle structures were observed by AFM (Fig. 7) within the first few minutes of emulsion preparation. Micelles showed ribbon-like structures that formed at the interface between water and oil (Fig. 7) indicating that self-assembly occurred at the very early stages of the experiments. However, initially ribbons were rather short ( $<250\text{ nm}$ ) and scarce. Longer ribbons were observed with continued incubation, while at the same time short ribbons appeared and the overall number of ribbons increased with time. This indicates

that ribbons elongate gradually over time and new ribbons form when further amelogenin molecules are released from the metastable micelle surface.

The formation of a reverse micelle exposes the hydrophobic portion of rH174 on the micelle surface and allows for intermolecular interaction between amelogenin molecules at the hydrophobic end. In the model of Fig. 8 we propose that extension of the hydrophobic core into the oil phase allows for intermolecular interaction of this portion of the amelogenin molecules that usually tends to fold inwards when exposed to polar solvents. At this point we hypothesize that initially dimers form when amelogenin coated reverse micelles approach each other. Such dimers stabilize through the formation of hydrogen bonds or van der Waals and electrostatic forces and along the hydrophobic portion of the molecule which contains large numbers of glutamate and histidin residues. Repetition of short sequences often are associated with supramolecular and fibrillar self-assembly in peptides. In this regards, the repeating triplets of glu-pro-xxx between position 108 and 130 constitute a unique sequence within the primary structure of rH174 and may present a suitable candidate for intermolecular bonds and the formation of anti-parallel  $\beta$ -sheets. A similar sequence of the bovine amelogenin protein has been synthesized and studied by Renugopalakrishnan et al (Renugopalakrishnan, 2002). He proposed the presence of  $\beta$ -spirals for this sequence which form channels for calcium ion transport (Renugopalakrishnan et al., 1989). A link between the numbers of repeating triplets PXX/PXQ in amelogenins and the resulting apatite crystal dimensions in enamel from different animals has been suggested previously, indicating its relevance to amelogenin self-assembly (Jin et al., 2009). Since reverse micelles are considered, the model further suggests that the N-terminal portions and the hydrophobic core of two amelogenin molecules interact to form stable bonds resulting in the hydrophilic c-termini being oriented towards the outside of the ribbons. The significant spacing of at least 10 to 30 nm suggest that these ribbons repulse each other due to electrostatic charges as shown in TEM images (Figs. 2 to 5) which supports the hypothesis that the charged hydrophilic domain is located towards the sides of the ribbons. Within the primary structure of amelogenin, the c-terminus shows the highest density of charged amino acids. Further analysis of the detailed molecular arrangement is currently underway using antibody staining and cryo-TEM.

The study also revealed that both calcium and phosphate ions must be involved to facilitate the self-assembly process into amelogenin ribbons. We have not been able to precisely identify the location of these ions within the ribbons using EELS for calcium or phosphate detection. The presence of a dark central line that runs along the ribbon long axis visible in the TEM (Figs. 1 and 5) is an indication of increased electron density and can be attributed to the presence of larger ions like calcium and phosphate. The degree of saturation of the ionic solutions used during self-assembly is in the metastable range and thus high enough to facilitate apatite precipitation. The study, however, could not identify the formation of a calcium phosphate mineral phase using TEM, SEM or Raman-spectroscopy. SEM-EDX showed small amount of calcium and phosphate are most likely bound in ionic form to the protein. Calcium ions are well known for its role in self-assembly for several proteins and peptides. The bivalent calcium ion can form bridges and facilitate bonds between two macromolecules. Calcium ions may play a similar role in the assembly of amelogenin nanoribbons. In contrast to other system amelogenin self-assembly into nanoribbons may require both the presence of calcium and phosphate ions, since approaches to generate ribbons in the absence of phosphate but in the presence of calcium failed. The presence of phosphate for supramolecular assembly is unique and has not been reported previously. Further investigations are warranted to identify both calcium and phosphate binding sites and their effect on self-assembly and folding.



The refolding of the recombinant protein may be a critical aspect of amelogenin studies performed in-vitro. To obtain the recombinant protein, amelogenin undergoes several harsh treatments including the use of several solvents and exposure to low pH solutions and lyophilization. Reconstitution of the protein to its native state by resuspension in aqueous buffered solutions may not be as straightforward as previously thought. Correct refolding of a protein from a denatured state to an ordered biologically active state is a complex process since intermediate structures can form and be stable under certain conditions (Lamba et al., 2009). There have been attempts to use hydrophobic surfaces to understand folding of proteins. Refolding experiments are usually designed for non-structural proteins with well defined functions, e.g. signaling or ligand-binding. Structural proteins, which are often fibrillar like collagen, fibrogen, and elastin, require self-assembly and often hierarchical self-assembly in order to obtain functionality. Conversely, it has been shown that several amyloidogenic proteins self-assemble into fibrils via a mechanism known as domain swapping. In domain swapping, proteins are proposed to undergo partial unfolding followed by recombination in an oligomeric state via reciprocal exchange of a structural element or domain (Nagarkar et al., 2010). The formation of  $\beta$ -sheets has frequently been mentioned as a possible motif of amelogenin folding related to self-assembly. Studies by Renupolokrishnan et al. suggested the formation of  $\beta$ -spirals in amelogenin aggregates that channel calcium ions to the apatite crystallization site (Renugopalakrishnan et al., 1989). Micro-Raman spectroscopy was performed in the present study on lyophilized powder of rH174 and self-assembled amelogenin nanoribbons. The obtained spectra showed a shift of the amide I bands towards higher wavenumbers with a sharp peak at  $1671\text{ cm}^{-1}$ . As shown for several peptides and proteins, such shift correlates with an increase of components that have  $\beta$ -sheet motif and may be associated with an anti-parallel orientation of strands that make up extended  $\beta$ -sheet assembly (Kubelka and Keiderling, 2001). Helical components tend to show maximum of amide I bands at  $1650\text{ cm}^{-1}$  and are reduced after ribbon formation. A previous study also reported that an increase in protein concentration may trigger a structural transition from PPII/unordered to  $\beta$ -sheet (Lakshminarayanan et al., 2007). The peak at  $1608\text{ cm}^{-1}$  observed in spectra of nanoribbons is characteristic of  $\beta$ -sheets and further corroborates the notion of  $\beta$ -sheets being a significant component of the assembled structures. Nevertheless reminiscence of a band around  $1640\text{ cm}^{-1}$  also indicates the presence of random coil structure after assembly. Overall the current Raman spectroscopic analysis suggests, comparable protein motifs are present in the lyophilized system and amelogenin nanoribbons, however  $\beta$ -sheet formation appears to become more prevalent and dominates the structure after ribbon formation.

A model of ribbon development and growth is shown in Figure 8 and is primarily based on the presence of amelogenin dimers which initially form when the reverse micelles connect with each other. The dimers are released when the micelles disintegrate due to the metastability of the emulsions. Phase separation and decomposition of the reverse micelles are therefore a requirement for amelogenin nanoribbon formation. Hence ribbons form at a faster rate and are much more abundant in emulsions prepared at pH 4.5. Reverse micelles contain water and have a higher density as the surrounding oil phase and gradually sink downwards in the microemulsion system. They decompose at the water-oil interface by releasing the water content into the water layer, which gradually rises over time. At this point the amelogenin molecules in the form of dimers orient themselves at the interface with the hydrophilic portion of the molecule immersed in the water phase while the hydrophobic portion is surrounded by the oil phase above the water phase (Fig. 8c). There also must be numerous amelogenin molecules that have not been paired yet with another molecule. Such monomers will also accumulate at the oil-water interface and are oriented in a similar fashion with the c-terminal localized in the polar phase. These oriented molecules are also able to form dimers as those formed directly from the reverse micelles. The amelogenin dimers are able connect to each other at their front and back, but will repulse each other at

the charged sides. Gradually short ribbon segments form, which can connect to each other to form longer ribbons. When ribbons reached a certain length, will eventually become dense and heavy enough to sink down into the water phase and to the bottom of the test tubes. Such ribbons were detected by the time-resolved DLS analysis as larger particle at day 6 and 7 (Fig. 1d). The repulsive forces at the edges not only keep the molecules from agglomerating randomly, but also gradually push the ribbons into parallel alignment. High degree of alignment of nanofibers from amphiphiles has recently been reported and attributed to the presence of charged domains at the fibril surface when exposed to x-ray radiation (Cui et al., 2010).

The observation of self-aligning amelogenin structures seems in particular important when considering the role of the observed nanoribbon formation of amelogenin for the organized crystallization of apatite in dental enamel. A challenge in the current model of enamel maturation is a lack of our understanding of how enamel matrix proteins can achieve the high degree of organization of apatite crystals on a nanometer scale. Apatite nanofibers of 50 nm diameter and several hundreds of micrometer length are packed in a predominantly parallel fashion into enamel rods. The possibility of amelogenin forming nanoribbons that align themselves in a parallel fashion may provide a possible model on how amelogenin can guide apatite crystal growth in enamel. It is feasible that apatite grows uniaxially along oriented ribbons of amelogenin following a line of calcium and phosphate ions at the ribbons' central axes. Amelogenin nanoribbons would continue to elongate as more protein is expressed by the ameloblast and crystal growth continues at the same rate as the ribbons grow. Apatite mineral has been reported to be ribbon-like at the early stages of enamel maturation (Glimcher, 1968). Enamel mineralization will be finalized when enamel matrix proteases, e.g. MMP-20 and KLK-4, remove amelogenin protein in a controlled fashion and allow lateral growth of the apatite crystals.

## Conclusions

This study developed a procedure that facilitated the interactions of the hydrophobic portion of the amphiphilic amelogenin molecule rH174 using a water in oil emulsion system. The methodology induced the formation of amelogenin nanoribbons which are a new form of supramolecular assembly of this enamel matrix protein that has not been described before. The nanoribbons require calcium and phosphate for assembly and are able to align themselves in a parallel fashion. The observed new supramolecular assembly of amelogenin may impact the current paradigm on protein guided enamel mineralization of highly oriented apatite nanocrystals.

## Acknowledgments

Financial Support by NIH/NIDCR grants RO1DE 017529 and RO1DE017529S2.

## References

- Aichmayer B, Margolis HC, Sigel R, Yamakoshi Y, Simmer JP, Fratzl P. The onset of amelogenin nanosphere aggregation studied by small-angle X-ray scattering and dynamic light scattering. *J Struct Biol.* 2005; 151:239–49. [PubMed: 16125972]
- Aichmayer B, Wiedemann-Bidlack FB, Gilow C, Simmer JP, Yamakoshi Y, Emmerling F, Margolis HC, Fratzl P. Amelogenin nanoparticles in suspension: Deviations from spherical shape and pH-dependent aggregation. *Biomacromolecules.* 2010; 11:369–76. [PubMed: 20038137]
- Beniash E, Simmer JP, Margolis HC. The effect of recombinant mouse amelogenins on the formation and organization of hydroxyapatite crystals in vitro. *J Struct Biol.* 2005; 149:182–90. [PubMed: 15681234]

- Berne BJ, Pecora R. Laser Light-Scattering from Liquids. *Annual Review of Physical Chemistry*. 1974; 25:233–253.
- Chen Y, Wu QS, Dingibi Y. Stepwise assembly of nanoparticles, -tubes, -rods, and -wires in reverse micelle systems. *European Journal of Inorganic Chemistry*. 2007:4906–4910.
- Choi IS, Bowden N, Whitesides GM. Macroscopic, Hierarchical, Two-Dimensional Self-Assembly. *Angew Chem Int Ed Engl*. 1999; 38:3078–3081. [PubMed: 10540428]
- Claussen RC, Rabatic BM, Stupp SI. Aqueous self-assembly of unsymmetric Peptide bolaamphiphiles into nanofibers with hydrophilic cores and surfaces. *J Am Chem Soc*. 2003; 125:12680–1. [PubMed: 14558795]
- Colfen H, Mann S. Higher-order organization by mesoscale self-assembly and transformation of hybrid nanostructures. *Angew Chem Int Ed Engl*. 2003; 42:2350–65. [PubMed: 12783497]
- Cui H, Pashuck ET, Velichko YS, Weigand SJ, Cheetham AG, Newcomb CJ, Stupp SI. Spontaneous and x-ray-triggered crystallization at long range in self-assembling filament networks. *Science*. 2010; 327:555–9. [PubMed: 20019248]
- Elie-Caille C, Fliniaux O, Pantigny J, Maziere JC, Bourdillon C. Self-assembly of solid-supported membranes using a triggered fusion of phospholipid-enriched proteoliposomes prepared from the inner mitochondrial membrane. *Langmuir*. 2005; 21:4661–8. [PubMed: 16032886]
- Fan Y, Sun Z, Wang R, Abbott C, Moradian-Oldak J. Enamel inspired nanocomposite fabrication through amelogenin supramolecular assembly. *Biomaterials*. 2007; 28:3034–42. [PubMed: 17382381]
- Fincham AG, Moradian-Oldak J, Diekwisch TG, Lyaruu DM, Wright JT, Bringas P Jr, Slavkin HC. Evidence for amelogenin “nanospheres” as functional components of secretory-stage enamel matrix. *J Struct Biol*. 1995; 115:50–9. [PubMed: 7577231]
- Frank J, Radermacher M, Penczek P, Zhu J, Li Y, Ladjadj M, Leith A. SPIDER and WEB: processing and visualization of images in 3D electron microscopy and related fields. *J Struct Biol*. 1996; 116:190–9. [PubMed: 8742743]
- Glimcher MJ. Recent Studies of Early Mineral Deposits in Bone and Enamel and of Organic Matrix of Enamel. *Calcified Tissue Research S*. 1968; 2:1.
- Habelitz S, Kullar A, Marshall SJ, DenBesten PK, Balooch M, Marshall GW, Li W. Amelogenin-guided crystal growth on fluoroapatite glass-ceramics. *J Dent Res*. 2004; 83:698–702. [PubMed: 15329375]
- Hartgerink JD, Beniash E, Stupp SI. Self-assembly and mineralization of peptide-amphiphile nanofibers. *Science*. 2001; 294:1684–8. [PubMed: 11721046]
- He X, Li W, Habelitz S. The cooperative self-assembly of 25 and 23kDa amelogenins. *J Struct Biol*. 2008; 164:314–21. [PubMed: 18845261]
- Jin T, Ito Y, Luan X, Dangaria S, Walker C, Allen M, Kulkarni A, Gibson C, Braatz R, Liao X, Diekwisch TG. Elongated polyproline motifs facilitate enamel evolution through matrix subunit compaction. *PLoS Biol*. 2009; 7:e1000262. [PubMed: 20027208]
- Kelley BD, Wang DI, Hatton TA. Affinity-based reversed micellar protein extraction: I. principles and protein-ligand systems. *Biotechnol Bioeng*. 1993; 42:1199–208. [PubMed: 18609669]
- Kubelka J, Keiderling TA. Differentiation of beta-sheet-forming structures: ab initio-based simulations of IR absorption and vibrational CD for model peptide and protein beta-sheets. *J Am Chem Soc*. 2001; 123:12048–58. [PubMed: 11724613]
- Kwak SY, Wiedemann-Bidlack FB, Beniash E, Yamakoshi Y, Simmer JP, Litman A, Margolis HC. Role of 20-kDa amelogenin (P148) phosphorylation in calcium phosphate formation in vitro. *J Biol Chem*. 2009; 284:18972–9. [PubMed: 19443653]
- Lakshminarayanan R, Fan D, Du C, Moradian-Oldak J. The role of secondary structure in the entropically driven amelogenin self-assembly. *Biophys J*. 2007; 93:3664–74. [PubMed: 17704165]
- Lamba J, Paul S, Hasija V, Aggarwal R, Chaudhuri TK. Monitoring protein folding and unfolding pathways through surface hydrophobicity changes using fluorescence and circular dichroism spectroscopy. *Biochemistry*. 2009; 48:393–8. [PubMed: 19463092]
- Lefevre T, Rousseau ME, Pezolet M. Protein secondary structure and orientation in silk as revealed by Raman spectromicroscopy. *Biophys J*. 2007; 92:2885–95. [PubMed: 17277183]

- Leunissen ME, van Blaaderen A, Hollingsworth AD, Sullivan MT, Chaikin PM. Electrostatics at the oil-water interface, stability, and order in emulsions and colloids. *Proc Natl Acad Sci U S A*. 2007; 104:2585–90. [PubMed: 17307876]
- Li W, Gao C, Yan Y, DenBesten PK. X-linked amelogenesis imperfecta may result from decreased formation of tyrosine rich amelogenin peptide (TRAP). *Arch Oral Biol*. 2003; 48:177–183. [PubMed: 12648554]
- Lindoy, LF.; Atkinson, IM. *Self-assembly in Supramolecular. Systems* Royal Society of Chemistry; Cambridge, UK: 2000.
- Ludtke SJ, Baldwin PR, Chiu W. EMAN: semiautomated software for high-resolution single-particle reconstructions. *J Struct Biol*. 1999; 128:82–97. [PubMed: 10600563]
- Margolis HC, Beniash E, Fowler CE. Role of macromolecular assembly of enamel matrix proteins in enamel formation. *J Dent Res*. 2006; 85:775–93. [PubMed: 16931858]
- Monnard PA, Deamer DW. Membrane self-assembly processes: steps toward the first cellular life. *Anat Rec*. 2002; 268:196–207. [PubMed: 12382318]
- Moradian-Oldak J. Amelogenins: assembly, processing and control of crystal morphology. *Matrix Biol*. 2001; 20:293–305. [PubMed: 11566263]
- Moradian-Oldak J, Paine ML, Lei YP, Fincham AG, Snead ML. Self-assembly properties of recombinant engineered amelogenin proteins analyzed by dynamic light scattering and atomic force microscopy. *J Struct Biol*. 2000; 131:27–37. [PubMed: 10945967]
- Nagarkar RP, Hule RA, Pochan DJ, Schneider JP. Domain swapping in materials design. *Biopolymers*. 2010; 94:141–55. [PubMed: 20091872]
- Nicholls A, Sharp KA, Honig B. Protein folding and association: Insights from the interfacial and thermodynamic properties of hydrocarbons. *Proteins*. 1991; 11:281–296. [PubMed: 1758883]
- Ohi M, Li Y, Cheng Y, Walz T. Negative Staining and Image Classification - Powerful Tools in Modern Electron Microscopy. *Biol Proced Online*. 2004; 6:23–34. [PubMed: 15103397]
- Qi L, Colfen H, Antonietti M, Li M, Hopwood JD, Ashley AJ, Mann S. Formation of BaSO<sub>4</sub> fibres with morphological complexity in aqueous polymer solutions. *Chemistry*. 2001; 7:3526–32. [PubMed: 11560323]
- Renugopalakrishnan V. A 27-mer tandem repeat polypeptide in bovine amelogenin: synthesis and CD spectra. *J Pept Sci*. 2002; 8:139–43. [PubMed: 11991203]
- Renugopalakrishnan V, Pattabiraman N, Prabhakaran M, Strawich E, Glimcher MJ. Tooth enamel protein, amelogenin, has a probable beta-spiral internal channel, Gln112-Leu138, within a single polypeptide chain: preliminary molecular mechanics and dynamics studies. *Biopolymers*. 1989; 28:297–303. [PubMed: 2720110]
- Robinson C, Fuchs P, Weatherell JA. The Appearance of Developing Rat Incisor Enamel Using a Freeze Fracturing Technique. *Journal of Crystal Growth*. 1981; 53:160–165.
- Sepassi K, Yalkowsky SH. Solubility prediction in octanol: a technical note. *AAPS PharmSciTech*. 2006; 7:E26. [PubMed: 16584157]
- Tan J, Leung W, Moradian-Oldak J, Zeichner-David M, Fincham AG. The pH dependent amelogenin solubility and its biological significance. *Connect Tissue Res*. 1998; 38:215–21. [PubMed: 11063029]
- Trivedi R, Kompella UB. Nanomicellar formulations for sustained drug delivery: strategies and underlying principles. *Nanomedicine*. 2010; 5:485–505. [PubMed: 20394539]
- Uskokovic V, Drogenik M. Reverse micelles: inert nano-reactors or physico-chemically active guides of the capped reactions. *Adv Colloid Interface Sci*. 2007; 133:23–34. [PubMed: 17400166]
- Uskokovic V, Castiglione Z, Cubas P, Zhu L, Li W, Habelitz S. Zeta-potential and particle size analysis of human amelogenins. *J Dent Res*. 2010; 89:149–53. [PubMed: 20040742]
- vanBuuren AR, Tieleman DP, deVlieg J, Berendsen HJC. Cosurfactants lower surface tension of the diglyceride/water interface: A molecular dynamics study. *Langmuir*. 1996; 12:2570–2579.
- Walsh D, Mann S. Fabrication of Hollow Porous Shells of Calcium-Carbonate from Self-Organizing Media. *Nature*. 1995; 377:320–323.

- Wiedemann-Bidlack FB, Beniash E, Yamakoshi Y, Simmer JP, Margolis HC. pH triggered self-assembly of native and recombinant amelogenins under physiological pH and temperature in vitro. *J Struct Biol.* 2007; 160:57–69. [PubMed: 17719243]
- Yan D, Zhou Y, Hou J. Supramolecular self-assembly of macroscopic tubes. *Science.* 2004; 303:65–7. [PubMed: 14704422]

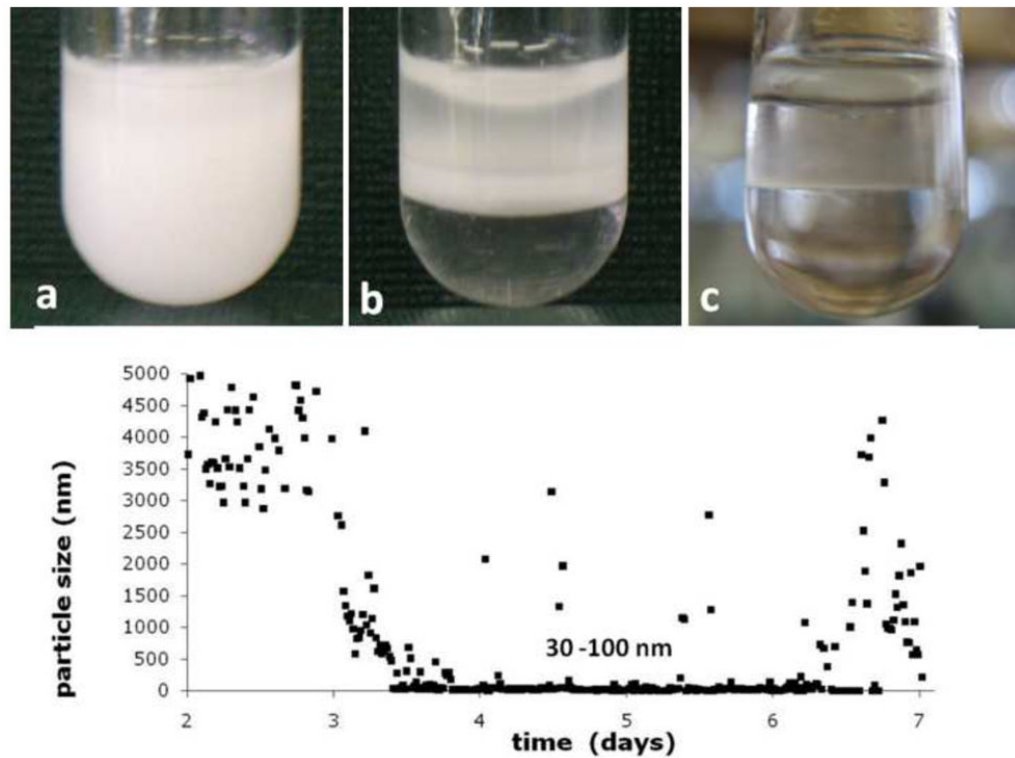


**Figure 1.** Emulsions of aqueous amelogenin suspensions form when mixed with Octanol/Ethylacetate in the presence of calcium and phosphate,  $t = 10$  min (a); emulsions prepared at pH 4.5 gradually phase separated into an oil and water phase,  $t = 3$  h (b) and are completely separated within 48 hours (c). Particle size analysis by time-resolved dynamic light scattering (d) (initial 48 hours not shown due to particle size being out of range) shows a decrease after 2 days from micrometer sized particles to sizes of 30 – 100 nm followed by fluctuations in particle sizes with particles reaching several micrometers in diameter at 6–7 days of incubation at  $37^{\circ}\text{C}$ .

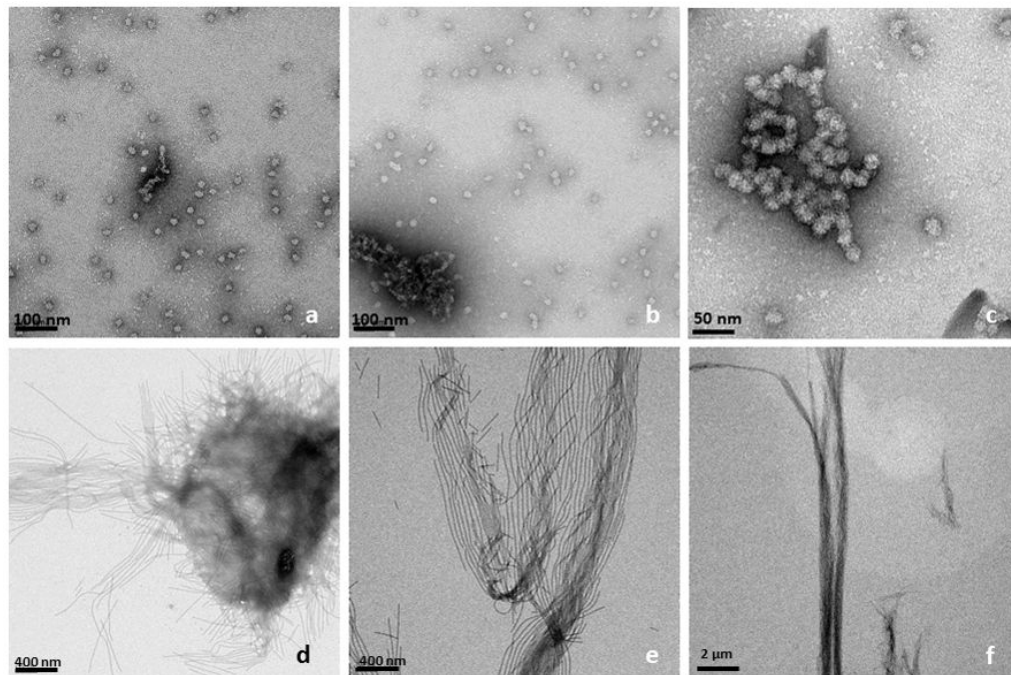


**Figure 2.**

TEM-images of amelogenin rH174 at different times of incubation; top row (a–c) rH174 was dissolved in aqueous suspensions at pH 2–3, subsequently pH was raised 4.5 using KOH and Tris-buffer. The characteristic 20 nm nanosphere of amelogenin was observed at all time points between 1 to 14 days of incubation,  $t = 24$  h (a); occasionally nanosphere aggregated into short strings,  $t = 48$  h (b), and  $t = 7$  days (c). When aqueous amelogenin suspensions were mixed at pH 2–3 with a non-polar solvent (octanol/ethyl acetate) and subsequently pH was raised to 4.5, ribbon-like nano-structures appeared as early as 24 hours (d). Ribbons grew in length over time and arranged themselves in a parallel manner,  $t = 7$  days (e); ribbons reached several micrometer in length and formed well aligned bundles of nanoribbons,  $t = 14$  days (f).

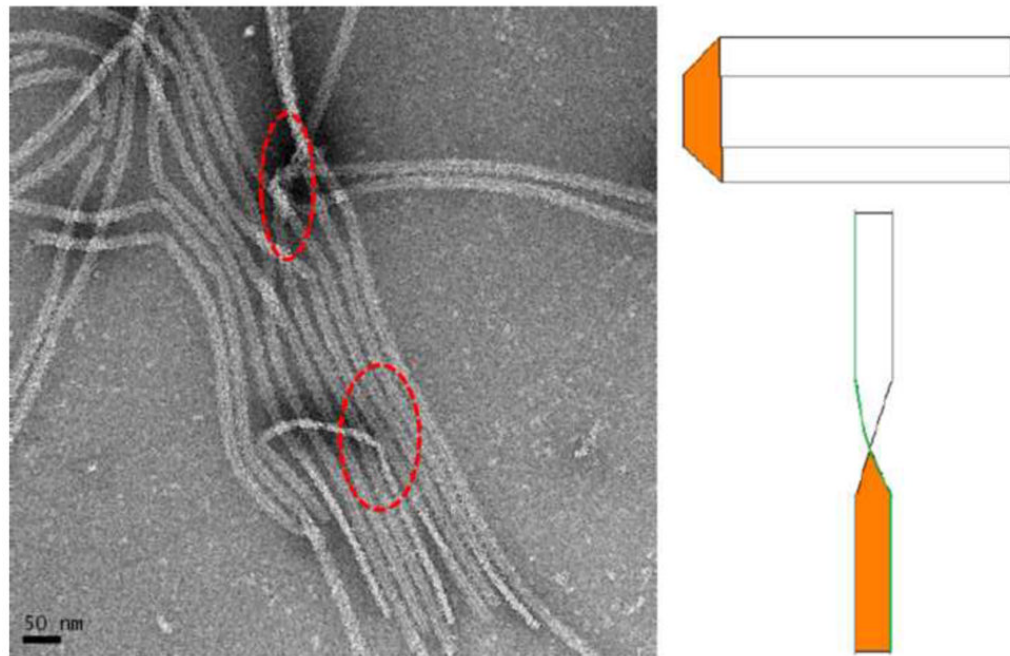


**Figure 3.**

TEM analysis of self-assembled amelogenin supramolecular structure showed that structures are about 17 nm wide and are thin ribbons, only 3 nm thick. The structures tend to align themselves in a parallel fashion, most likely through electrostatic repulsion at the long axes of the ribbons.



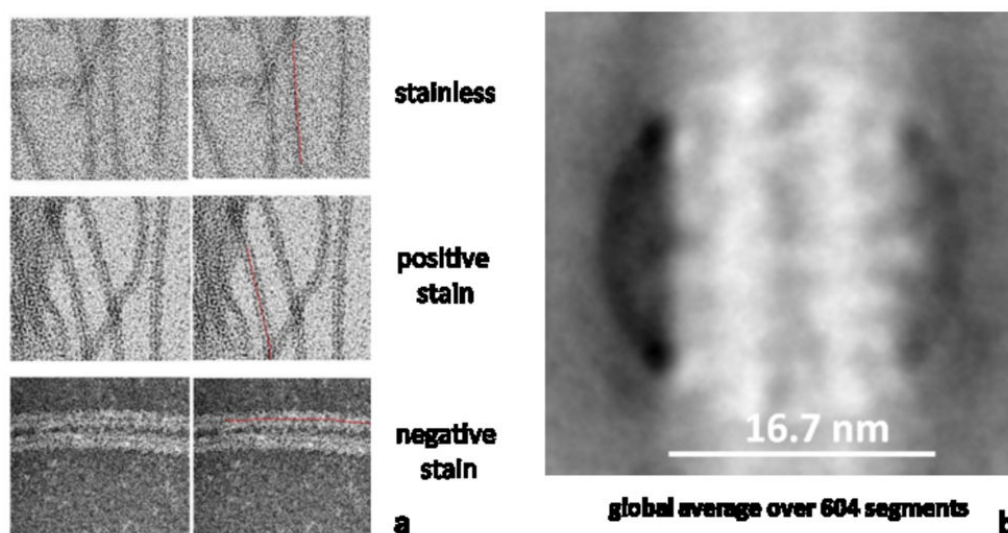


**Figure 4.**

TEM analysis of amelogenin nanoribbons showed the presence of a dark central line which was present in the absence of stain and when specimens were positively or negatively stained with nano-W (a). Averaging over 604 equally sized ribbon segments (negative stain) further revealed the evidence of a dark central line that indicated higher electron density which could be associated with the presence of calcium and/or phosphate ions which were both required for self-assembly into ribbons.

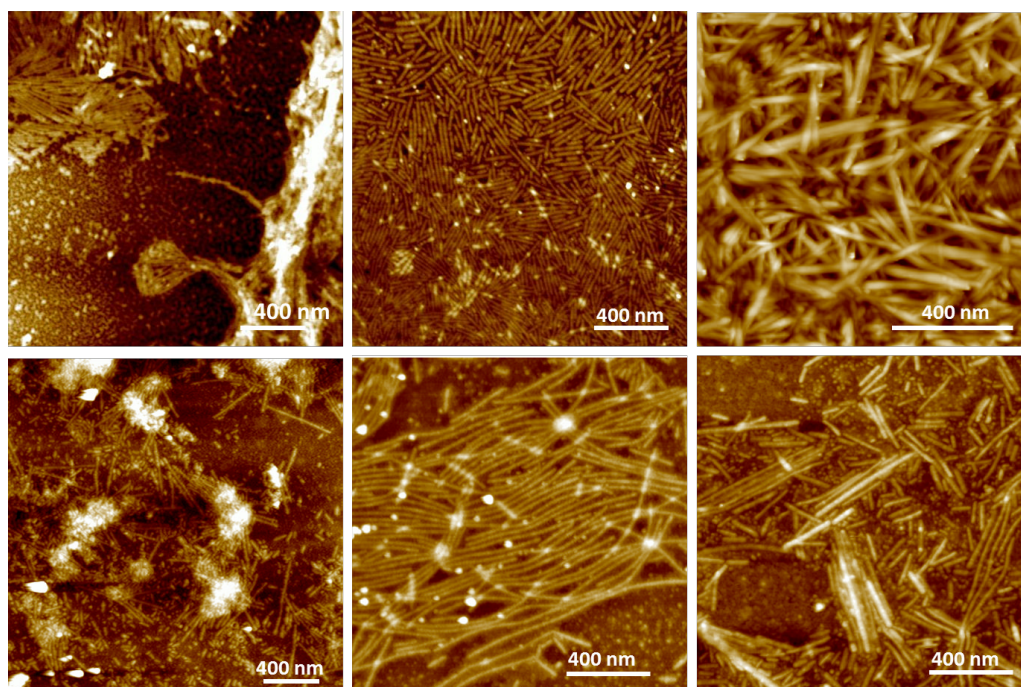


**Figure 5.** AFM topographic images (tapping mode) of a series of amelogenin nanostructures that formed at pH 4.5 (a–c) or pH 7.4 (d–f). Ribbons were observed as early as 30 min after emulsion formation at pH 4.5 (a), while ribbons appeared after 3 days at pH 7.4 (d). Ribbons became more abundant with time at pH 4.5, at 7 days (b) and at 14 days (c) while ribbons remained scarce at pH 7.4.

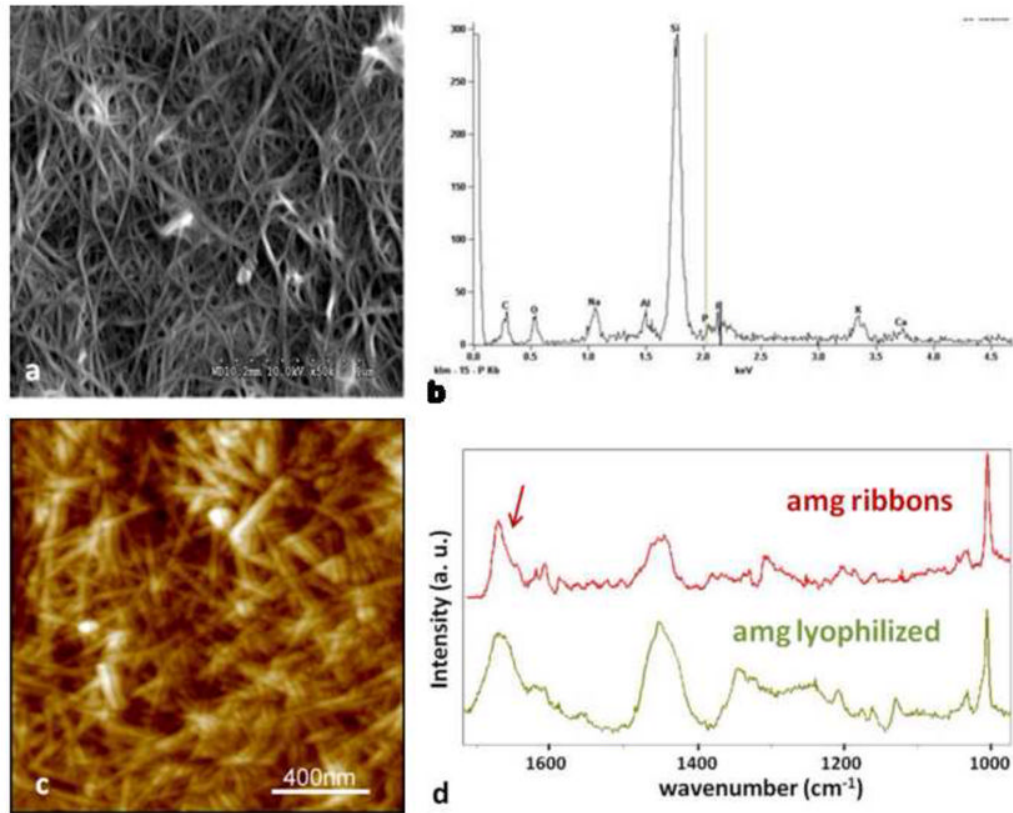


**Figure 6.**

Large amounts of amelogenin ribbons were observed by SEM (a) and elemental analysis by EDX confirmed the presence of small amounts of Calcium and Phosphate ions in these structures which were deposited onto a silica based microscope slide (b). The more randomly distributed ribbons were also observed by AFM but only in areas where large amounts of the protein could be immobilized to the glass surface (c). Analysis of the fibrillar structures using micro-Raman spectroscopy showed large similarities between the lyophilized amelogenin powder as received after purification and the self-assembled structures deposited onto a glass-slide. Overall the spectrum obtained from the amelogenin ribbons appeared more pronounced with respect to the amide vibrational modes above 1400  $\text{cm}^{-1}$ . In particular the sharpening of a band at 1670  $\text{cm}^{-1}$  and the occurrence of a band around 1610  $\text{cm}^{-1}$  are indicative of the formation of  $\beta$ -sheet structures.

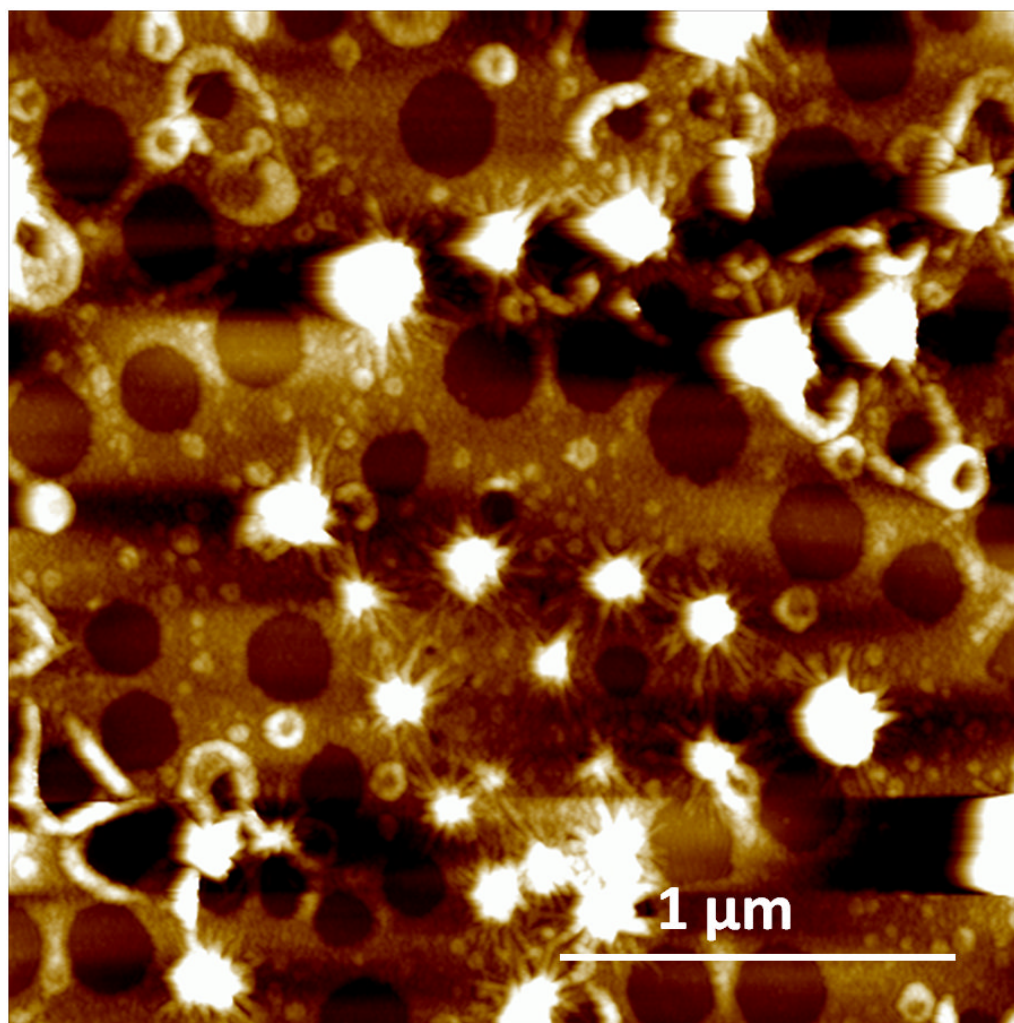


**Figure 7.** AFM image of micellar structures that are present at the early time points of emulsification. Sample obtained at 5 min after vortexing.

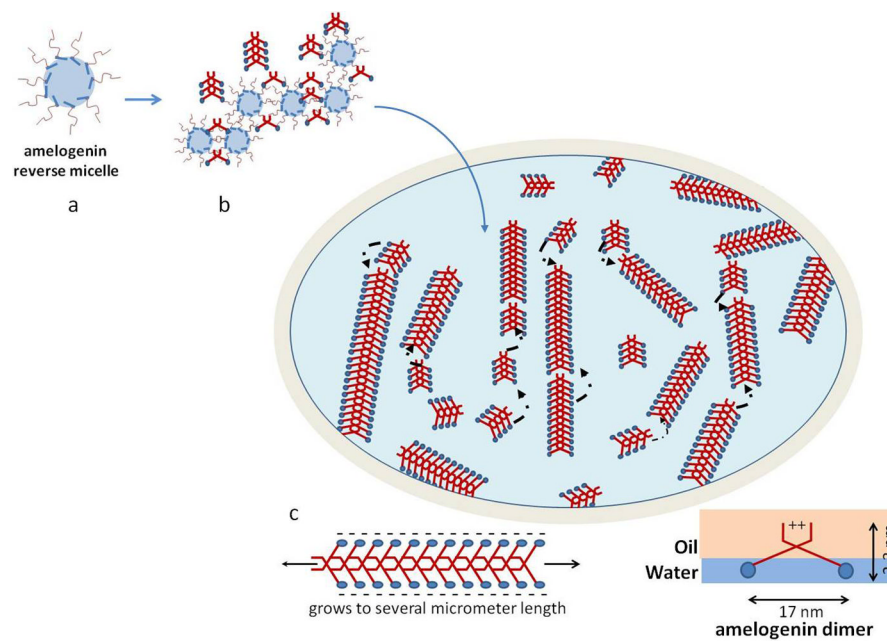


**Figure 8.**

Schematic drawing of the possible supramolecular structure of amelogenin nanoribbons that form at the oil-water interface. Initially a reverse micelle forms with the hydrophobic portion of the molecules (red) exposed to the surface. The hydrophobic portions can now interact with each other and form unique bonds that are most likely based on calcium bridges and Van der Waals bonds and lead to the formation of structural motifs like  $\beta$ -sheets. Such amelogenin dimers will grow by the addition of other dimers that are released from the reverse micelles soon as these micelles disintegrate at the water-oil interface. Gradually ribbons will form by addition of segments to its ends. Segments repulse each other at the long axis to electrostatic charges that derive from the hydrophilic portion (blue) lining the long axis of the ribbons. Electrostatic repulsion will result in parallel alignment of ribbons over time and also facilitates oriented grows of ribbons along their long axes.